Positron annihilation and binding in aromatic and other ring molecules

E. Arthur-Baidoo [*], J. R. Danielson [†] and C. M. Surko [‡]

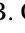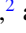*Physics Department, University of California San Diego, La Jolla, California 92093 USA*

J. P. Cassidy [1], S. K. Gregg [1], J. Hofierka [1], B. Cunningham [1], C. H. Patterson [2], and D. G. Green [1,§]

[1]*Centre for Light-Matter Interactions, School of Mathematics and Physics, Queen's University Belfast,*
University Road, Belfast BT7 1NN, Northern Ireland, United Kingdom
[2]*School of Physics, Trinity College Dublin, Dublin 2, Ireland*

Measured annihilation spectra are presented for aromatic and heterocyclic ring molecules resolved as a function of incident positron energy using a trap-based positron beam. Comparisons with the vibrational mode spectra yield positron-molecule binding energies. *Ab initio* many-body theory predictions, which take proper account of electron-positron correlations including virtual-positronium formation, are presented and are found to be in good to excellent agreement with the measured binding energies. The calculations elucidate the competition between permanent dipole moments and π bonds in determining the spatial distribution of the bound-state positron density. The implications of these results and the role of multimode features in annihilation in these molecules, including Fermi resonances, are discussed.

I. INTRODUCTION AND OVERVIEW

Positrons bind to many polyatomic molecules via the excitation of vibrational Feshbach resonances (VFRs) [1–3]. Binding energies for >100 molecules have been measured to date with magnitudes ranging from a few millielectron volts to >0.3 eV. While positrons are also predicted to bind to atoms [4–6], they have yet to be observed experimentally due to the lack of low-lying excitations to mediate attachment, though proposals exist [7–10]. Thus, molecular studies play a special role in our understanding of positron interactions with matter.

Experimentally, positron binding has been observed to depend upon molecular parameters such as the polarizability α, permanent dipole moment μ, the number of molecular π bonds N_π, the ionization potential I, and the geometry (e.g., as seen in isomers) [11–15]. For unsaturated ring molecules, enhancement of the positron-molecule binding energy ε_b with increasing N_π is observed [15].

Theoretical work has successfully predicted many aspects of these chemical trends, but there remain a number of important questions [13,16–21]. Scattering calculations using model potentials have also been used to estimate binding energies for benzene and several ring molecules like those studied here [22–26].

A recent many-body theory (MBT) [27] developed by some of us provides an *ab initio* description of positron binding to molecules, importantly taking proper account of

electron-positron correlations including the nonperturbative process of virtual-positronium formation (where a molecular electron temporarily tunnels to the positron). To date, it has, e.g., provided calculated binding energies in agreement with measurements, quantified the role of correlations and the contributions of individual molecular orbitals to the positron-molecule correlation potential, and explained trends within molecular families [19,27]. It has recently been extended to positron scattering and annihilation on small molecules [28] and to calculations of positronic-bonded molecular dianions [29]. Particularly relevant to this paper, the MBT provides insights through calculations of the spatial distribution of the bound-state positron wave functions.

In this paper, measurements of the positron annihilation spectra and binding energies are presented for aromatic and substituted ring molecules and are compared with predictions of the MBT. We extend earlier studies [11,14,15] using ring substitutions to study molecules with a range of permanent dipole moments and numbers of π bonds. As a result, the molecules in this paper provide a sensitive test of the competition between their effects in positron binding. Results are presented for benzene, toluene, acetophenone, aniline, phenylacetylene, benzonitrile, benzaldehyde, furan, pyrrole, pyridine, pyridazine, cycloheptatriene (CHT), and cyclooctatetraene (COT). The molecules studied span a wide range of N_π (2–5), μ (0.3–4.5 D), and α (8–14 Å³). Good to excellent agreement is found between the MBT predictions and binding energy measurements for this group of molecules.

As discussed below, the MBT shows that regions of the bound-state positron density are localized near the π-bond *electron density* above and below planes of ring molecules such as benzene and toluene. This exemplifies the importance of the π bonds in localizing the bound-state positron wave

---

[*]earthurbaidoo@ucsd.edu

[†]jdan@physics.ucsd.edu

[‡]csurko@physics.ucsd.edu

[§]d.green@qub.ac.uk

062801-1

function. Other distributions of positron density are localized close to strong permanent dipole moments that typically lie in the planes of ring molecules such as in benzaldehyde and pyridine. For molecules with weaker dipole moments, including furan and pyrrole, the effects compete, and the bound-state positron distribution is observed in regions of both the π-bond electrons and adjacent to the negative end of the dipole. This contrasts with the approximately uniform covering of positron density surrounding nonpolar molecules without π bonds such as that seen in alkanes [16].

Positron annihilation rates for molecules are conventionally expressed in terms of the quantity Z_{eff}, which is the measured rate normalized by that expected for a gas of free electrons with the density equal to the density of the molecular gas [2]. Positron attachment via VFR typically results in annihilation rates $Z_{\text{eff}} \geqslant 10^3$ and greater than those expected for a simple collision (e.g., $Z_{\text{eff}} \simeq$ the number of valence electrons) [2]. The VFR theory of positron annihilation due to dipole- and quadrupole-allowed fundamental vibrations can account for enhancements of an order of magnitude or so in annihilation rate (e.g., $Z_{\text{eff}} \leqslant 2000$ for a single vibrational mode) [30,31]. However, Z_{eff} for many molecules, including those studied here, is 2–3 orders of magnitude larger, and this is not understood.

Of note in this paper and like that observed previously in benzene [32], broad regions in the annihilation spectra are observed in aromatic molecules such as pyridine and aniline at incident positron energies that do not correspond to fundamental vibrations. The origins of these features are likely multimode vibrations [21,33,34], where the specific modes involved have yet to be identified. Related to this, enhanced annihilation is observed in benzaldehyde that is likely due to the multimode phenomenon of Fermi resonance (FR, the resonance of a fundamental vibration with the second harmonic of another vibration). This provides an example of a multimode contribution to the annihilation spectrum where the specific modes involved are known and is worthy of further study.

This paper is organized as follows. Section II presents the description of the experiment and data analysis procedures. Section III presents the measured annihilation spectra as a function of incident positron energy and the resulting binding energy analyses. Section IV describes the MBT and the predicted binding energies for the molecules studied here and comparison with the measurements. Further aspects of the results are discussed in Sec. V, and Sec. VI presents a summary and concluding remarks.

II. DESCRIPTION OF THE EXPERIMENT AND DATA ANALYSIS

The experimental techniques used in this positron annihilation study have been described in detail previously [12]. Low-energy positrons are obtained from a ^{22}Na radioisotope source and a solid neon moderator. Positrons leaving the moderator are radially confined and guided using magnetic fields into a three-stage buffer-gas trap (BGT) [35]. In the BGT, they are slowed by inelastic collisions with N_2 and CF_4, resulting in positrons trapped and cooled to the ambient temperature (300 K). The pulsed positron beam is formed by slowly ramping the bottom of the potential well to a voltage

higher than that of the exit gate [12,35]. The beam thus formed has a narrow energy spread with a mean energy just slightly larger than the exit gate potential. The energy distribution of the beam is measured using a retarding potential analyzer.

For these experiments, the beam transport energy between the positron traps and annihilation cell is 0.67–0.70 eV. The *parallel* energy distribution of the beam is approximately Gaussian with a standard deviation $\sigma_{\parallel} = 8$–10 meV. The perpendicular energy of the beam is obtained from measuring mean parallel energy ($E_{\parallel}$) at different retarding potential analyzer magnetic fields. The slope of this measurement yields the mean perpendicular energy $E_{\perp} = 20 \pm 2$ meV [35]. The distribution in total energies is the convolution of the parallel and perpendicular energy distributions which yields an exponentially modified Gaussian (EMG) distribution [35]. The guiding magnetic field varies by a factor of five along the beam line, where the annihilation gas cell is located at the end [36]. The magnetic field at the gas cell is independently controlled. When it matches the value at the exit gate of the BGT, both the parallel and perpendicular particle distributions are known, and hence, the total energy distribution is known.

The positrons propagate downstream to a 26-cm-long gas cell, the potential of which is used to set the mean parallel energy of the beam interacting with the test gas. During annihilation measurements, an isolated electrode after the annihilation cell is biased to 6 V to reflect the beam back toward the BGT. Positrons continue to bounce between the exit gate of the BGT and the reflecting electrode while measurements are made. See Ref. [12] for details.

The measured annihilation rates are obtained by converting the annihilation counts (N_c) to an annihilation cross-section using the number of positrons per pulse (N_p), the calibrated detector efficiency (η_D), the test-gas density (n_m), and the annihilation cell length (L_D). For a given molecule, the normalized annihilation rate is given by [2]

$$Z_{\text{eff}}(E_{\parallel}) = \frac{N_c(E_{\parallel})}{2N_p \eta_D L_D n_m} \frac{\upsilon(E_{\parallel})}{\pi r_0^2 c},\tag{1}$$

where $\upsilon(E_{\parallel})$ is the mean particle velocity, r_0 is the classical radius of the electron, and c is the speed of light. The factor of two in the denominator accounts for the two passes of the positrons through the annihilation cell in a single bounce.

Shown in Fig. 1 is a recent measurement of Z_{eff} for the alkane octane plotted as a function of the mean parallel energy of the beam. The main features of this and most other measured spectra in this paper are VFRs associated with the C-H stretch vibrational modes at energies $\sim$0.36 eV. Also shown in Fig. 1 is the downshifted infrared (IR) absorption spectrum (henceforth referred to as the IR spectrum) arbitrarily scaled [37], which demonstrates the spread of the vibrational modes. The Z_{eff} spectrum shows an asymmetric resonant peak at $E_{\parallel} \approx$ 0.2 eV. To obtain the binding energy, a fit to the C-H stretch resonance is performed where each IR-active mode is taken to be a delta function and convolved with the beam EMG distribution. The resonances from all modes are summed to give a single resonant peak with a width which is a combination of the measured beam parameters and energies of the vibrational modes. The positron-molecule binding energy ε_b is obtained using the total energy ε_r at which the resonance is observed
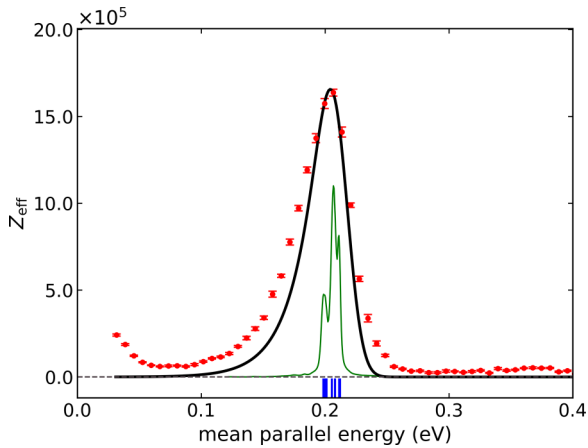
FIG. 1. Annihilation rate Z_{eff} for octane as a function of mean parallel energy of the positron beam. The green curve is the infrared (IR) spectrum of octane obtained from NIST [37], and vertical blue bars indicate the locations of the IR-active fundamental modes, with both downshifted by ε_b. The solid black line shows the fit to the C-H stretch modes used to determine ε_b.

and the vibrational mode energy $\hbar\omega$ with the relationship:

$$\varepsilon_b = \hbar\omega - \varepsilon_r. \quad (2)$$

For the octane data in Fig. 1, this procedure yields a binding energy of 150 ± 3 meV [12].

In contrast with octane and other alkane molecules [12], benzene and the other aromatics studied here have appreciable annihilation amplitudes that are believed to be due to unresolved multimode vibrational excitations [32]. This leads to uncertainty in obtaining the resonances used in Eq. (2). As a result, for all aromatic molecules, the choice was made to use only the dipole-active high-energy phenyl-CH stretch modes to obtain ε_b values. The modes used are shown as solid vertical lines in the figures, and the resulting fits are shown by the solid black lines. For most molecules, these fits match the data reasonably well. However, in a number of cases, including the other components of the spectra can modify the best-fit energy of the resonance by several meV. Thus, the conservative error estimate of ± 5 meV is associated with the ε_b measurements unless otherwise noted.

This analysis is based on the Gribakin and Lee (GL) theory for Z_{eff} from VFRs mediated by dipole-allowed fundamental vibrational modes [2,30]. If the IR activity for the fundamentals is known, and using ε_b obtained from above, the contribution from all modes can be added to predict the total expected Z_{eff} as a function of the mean parallel energy of the positron beam. For most molecular targets, this estimate is *much smaller* than that observed, while the spectral shape is often reasonably accurate. It is predicted that this behavior is due to single-mode vibrational excitations which function as doorways into multimode vibrations [38].

The amplitude of the fit can be related to the enhancement factor that the GL prediction must be multiplied by to match the measurements. For the molecules here, this factor varies from ∼220 for COT to ∼1.5 for furan. The solid line in Fig. 1 is 75 times the GL prediction for octane. This enhancement is believed to be due to the coupling of the fundamentals to many

multimode resonances by intramolecular vibrational redistribution (IVR) [2,39]. However, this has yet to be confirmed. The origin of this enhancement mechanism remains as a major topic of study, beyond the scope of this paper.

III. ANNIHILATION SPECTRA AND BINDING-ENERGY ANALYSES

In this paper, we focus on the manner in which additions to and substitutions in the benzene ring affect binding energies. The molecules studied can be grouped in three categories: (i) benzene (C_6H_6) and its derivatives, toluene ($-CH_3$), acetophenone ($-COCH_3$), phenylacetylene (–CCH), benzonitrile (–CN), and benzaldehyde (–CHO); (ii) the heterocyclic aromatic molecules furan, pyrrole, pyridine, and pyridazine; and (iii) nonaromatic cyclic molecules, CHT and COT. The results for each category and molecule are discussed separately. For easy referral during this discussion, the molecular parameters for all molecules and the measured positron-molecule binding energies are summarized in Table I.

A. Benzene and its substituted derivatives

A high-resolution annihilation spectrum for benzene was measured previously using the cryogenic trap-based beam, yielding $\varepsilon_b = 132 \pm 3$ meV [32]. However, to better compare with the other molecules, data from the room-temperature trap-based beam are shown in Fig. 2(a), along with the fit to the single dipole-allowed C-H stretch vibrational mode. As discussed in Ref. [32], an unusual feature of the spectrum is a broad range (i.e., $E_\parallel \sim 0.05\text{-}0.2$ eV) of enhanced annihilation in a region of energies absent of fundamental vibrational modes. As discussed below, these features appear to be quite common in aromatic molecules.

Benzene derivative molecules with side-group substitutions typically have dipole moments due to the addition or substitution. The new molecule with the smallest dipole moment studied here is toluene ($\mu = 0.33$ D), which consists of a benzene ring with an attached methyl (CH_3) group. It has three π bonds in the ring. While the net dipole moment of benzene is zero due to symmetry, the methyl group both creates a dipole moment and increases the polarizability of the molecule.

Shown in Fig. 2(b) is the annihilation spectrum of toluene. It has a sharp peak due to the five IR-active C-H stretch modes from benzene and three others from the methyl group that are visible in the IR spectrum [42]. The binding energy is found to be 173 ± 5 meV. The peak Z_{eff} value in toluene is ∼30 times greater than that in benzene, where the former is comparable with the enhancements seen in alkane molecules [12].

Shown in Fig. 2(c) is the annihilation spectrum of acetophenone. It is a benzene ring with an acetyl group (CH_3CO) attached, making it the simplest aromatic ketone. It has a peak Z_{eff} value of ∼3×10^6, which is the largest of all molecules in Table I. It has a net dipole moment of ∼3 D and four π bonds. Using the five phenyl and three methyl IR-active vibration modes [43], the binding energy is 288 ± 5 meV.

Aniline is an aromatic compound comprised of a benzene ring attached to an amide group (–NH_2). It has a net dipole moment of ∼1.5 D and three π bonds. Figure 2(d) shows the annihilation spectrum of aniline as a function of mean

TABLE I. Experimental (exp.) binding energies for the molecules studied, together with their molecular properties, polarizability (α) [40,41], dipole moment (μ) [40,41], number of π bonds (N_π), and ionization potential (I) [40,41]. The corresponding MBT calculated binding energies from this paper are shown in Table II.

Molecule	Structure	N_π	μ (D)	α (Å³)	I (eV)	ε_b (exp.) (meV)
Benzene and its substituted derivatives						
Benzene	C_6H_6	3	0.00	10	9.24	132 ± 3[a]
Toluene	$C_6H_5CH_3$	3	0.38	11.86	8.83	173 ± 5
Acetophenone	$C_6H_5COCH_3$	4	3.02	14.4	9.28	288 ± 5
Aniline	$C_6H_5NH_2$	3	1.53	12.1	7.72	233 ± 5
Phenylacetylene	C_6H_5CCH	5	0.66	13.8	8.82	230 ± 5
Benzonitrile	C_6H_5CN	5	4.52	12.5	9.73	298 ± 5
Benzaldehyde	C_6H_5CHO	4	3.14	12.80	9.50	220 ± 10
Heterocyclic aromatic molecules						
Furan	C_4H_4O	2	0.66	7.23	8.88	52 ± 5
Pyrrole	C_4H_4NH	2	1.77	7.9	8.2	165 ± 10
Pyridine	C_5H_5N	3	2.19	9.5	9.26	186 ± 5
Pyridazine	$C_4H_4N_2$	3	4.22	9.27	8.74	330 ± 10
Nonaromatic cyclic molecules						
Cycloheptane	C_7H_{14}	0	0.00	12.8	9.97	104 ± 4[b]
Cycloheptatriene (CHT)	C_7H_8	3	0.25	12.6	8.29	190 ± 8
Cyclooctane	C_8H_{16}	0	0.00	14.5	9.75	128 ± 4[b]
Cyclooctatetraene (COT)	C_8H_8	4	0.00	13.76	8.43	225 ± 5

[a]Value taken from Ref. [32].
[b]From Ref. [12]

parallel energy. There is an enhanced resonant peak at $E_\parallel \approx 0.2$ eV which is due to the phenyl C-H stretch modes. Using these modes, the resulting binding energy of aniline is 233 ± 5 meV. In comparison with toluene, both molecules show similar levels of enhancement of Z_{eff} (i.e., to within an order of magnitude). The difference in ε_b of ∼57 meV can likely be associated with the larger dipole moment in aniline. Like other aromatic molecules, the aniline spectrum displays broad spectral weight for $E_\parallel < 0.1$ eV. While the shoulder at $E_\parallel \approx 0.19$ eV on the high-energy side of the main peak is likely associated with the N-H stretch modes, the current energy resolution is not good enough to make a firm identification.

Phenylacetylene and benzonitrile were also studied. In the phenylacetylene molecule, one hydrogen on benzene is replaced with an alkyne, C≡C–H that includes a CC triple bond. In benzonitrile, one hydrogen is replaced with a cyanide (C≡N) group, which also includes a triple bond. Thus, both molecules have an additional two π bonds from the triple bonds, in addition to the three from the phenyl group, for a total of five π bonds. One difference, however, is that the net dipole of phenylacetylene ($\mu = 0.66$ D) is ∼6 times smaller than that of benzonitrile ($\mu = 4.52$ D).

Figure 2(e) shows the measured annihilation spectrum for phenylacetylene. Using the phenyl C-H stretch modes to define the resonant peak, $\varepsilon_b = 230 \pm 5$ meV. It is surprising that there is no obvious enhanced spectral feature that can be associated with the C-H stretch mode in the acetylene group, which lies ∼30 meV higher in energy than the C-H stretch mode in the phenyl ring. This is like the failure to observe a distinct feature for the N-H stretch modes in the spectra for aniline.

The annihilation spectrum of benzonitrile is shown in Fig. 2(f). Substitution of the highly polar C≡N group creates a net dipole moment of 4.5 D, which is the largest dipole mo-

ment of any molecule in this paper. Analysis using the phenyl C-H stretch modes yields $\varepsilon_b = 298 \pm 5$ meV. The enhanced ε_b value relative to phenylacetylene is likely associated with increased dipole moment.

Also considered in this group is benzaldehyde, which is benzene with an attached aldehyde (CHO) group, making it the simplest aromatic aldehyde. Substitution of the aldehyde group results in a relatively large dipole moment, $\mu = 3.14$ D [41,44]. The benzaldehyde molecule has a total of four π bonds, three from benzene and the fourth due to the C=O double (carbonyl) bond. The annihilation spectrum for benzaldehyde is shown in Fig. 3. The spectrum shows two large peaks that are not completely resolved, one at $E_\parallel \sim 0.1$ eV and one at $E_\parallel \sim 0.15$ eV. The peak at 0.15 eV is due to the phenyl C-H stretch modes.

The lower-energy peak is in the region of the aldehyde C-H stretch mode. However, for benzaldehyde, this mode is in a strong Fermi resonance [45] with the aldehyde C-H bend overtone. The result is two peaks with comparable amplitude, both of which are visible in the IR spectrum (cf. Fig. 3). The energy resolution of the 300 K beam is not sufficient to determine whether the annihilation resonance is from one or both modes, but including this spectral feature is necessary to determine ε_b.

The binding energy analysis used the vibrational frequencies of the two components of the FR and the C-H stretch vibrational modes from the phenyl group [45,46]. The result is $\varepsilon_b = 220 \pm 10$ meV. The larger error bar arises from the uncertainty in identifying the correct mode frequencies for use with Eq. (2). This value of ε_b for benzaldehyde is a factor of ∼1.7 times larger than that for benzene ($\varepsilon_b = 132$ meV; $\mu = 0$ D) and ∼1.2 times larger than that for toluene ($\varepsilon_b = 173$ meV; $\mu = 0.3$ D). The difference likely reflects the larger dipole moment of benzaldehyde. In contrast, the
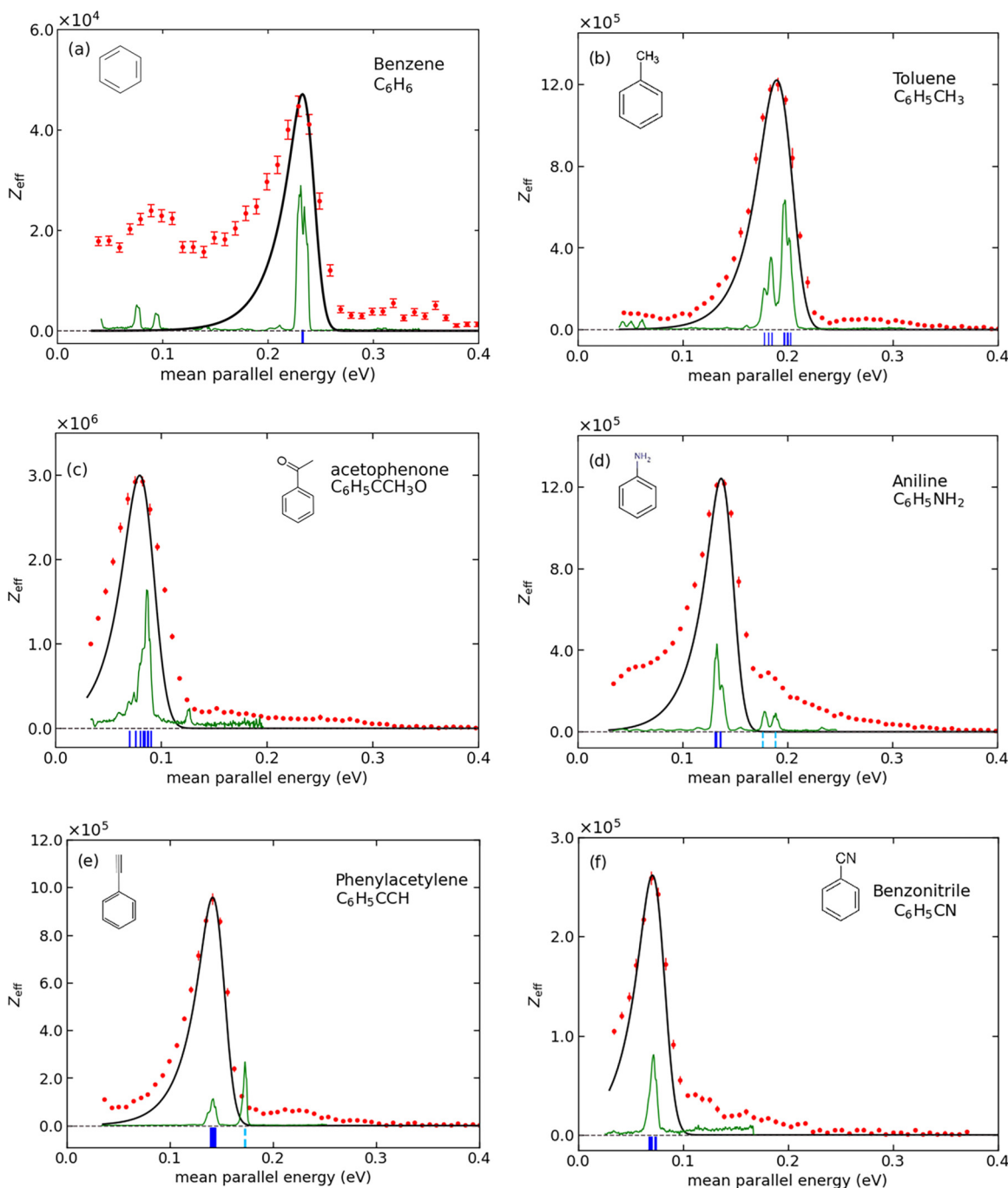
FIG. 2. Measured Z_{eff} values for benzene and its substituted derivatives (a) benzene, (b) toluene, (c) acetophenone, (d) aniline, (e) phenylacetylene, and (f) benzonitrile. The green curves are the infrared (IR) spectra obtained from NIST [37], and vertical blue bars indicate the locations of the IR-active fundamental modes, with both downshifted by ε_b. The solid black curves are fits to the C-H stretch peaks. Vertical dashed light blue lines indicate dipole-active fundamental modes not used in the analysis.

binding energy of benzaldehyde is a factor of $\sim$0.75 smaller than that of acetophenone ($\varepsilon_b = 288$ meV; $\mu = 3.0$ D), which has a comparable dipole moment but a larger α due to the added methyl group.

B. Heterocyclic aromatics

Four heterocyclic aromatic compounds were also studied: furan, pyrrole, pyridine and pyridazine. Heterocyclic molecules are compounds with at least two different atoms

in the ring. This can change the molecular polarizability and electronic structure, and it often adds a significant dipole moment.

Furan, which is the smallest heterocyclic aromatic, is a five-member ring composed of four carbon atoms and an oxygen. It has a dipole moment of 0.66 D. Figure 4(a) shows the Z_{eff} spectrum. It exhibits a broad set of resonances for $E_\parallel$ < 0.15 eV, and a well resolved peak at $E_\parallel \approx 0.33$ eV. This later peak is identified as due to the phenyl C-H stretch modes
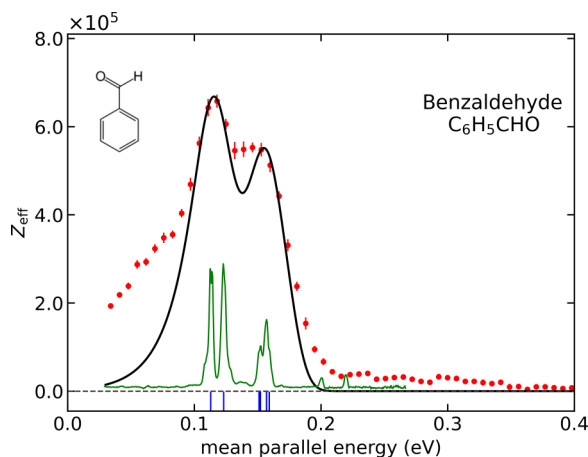
FIG. 3. Z_{eff} measurements for benzaldehyde. The green curves are the infrared (IR) spectra obtained from NIST [37]. The vertical blue bars at ~0.15 eV correspond to the C-H stretch modes of the phenyl ring, and those at 0.11–0.12 eV correspond to the Fermi resonance of the C-H stretch and the overtone of the C-H bend modes in the aldehyde group, with all downshifted by ε_b. The solid black curve is the fit (see text for details).

[47]. Using Eq. (2), $\varepsilon_b = 52 \pm 5$ meV. From comparison with the downshifted IR spectrum, the unresolved lower-energy resonances correspond to a large number of low-energy fundamental modes but were not analyzed in detail here. Such a spectrum is common for molecules with small ε_b values where the low-energy vibrational mode resonances are prominent [48].

Figure 4(b) shows the annihilation spectrum of pyrrole. Pyrrole is a five-member ring like furan but with the oxygen atom replaced by an N-H group. Like furan, pyrrole has two π bonds, but it has a larger dipole moment of 1.77 D. The most distinct peak is at $E_\parallel \approx 0.2$ eV which is identified with the four phenyl C-H stretch modes. The result is $\varepsilon_b = 165 \pm 10$ meV. Like benzene, pyrrole has significant annihilation over a broad energy range where there are no fundamental modes. This leads to a larger uncertainty in the fit and hence a larger error bar for ε_b. There is a small structure in the annihilation spectrum for $E_\parallel \approx 0.26$ eV that is likely associated with the single N-H vibration. This is consistent with the measured ε_b but was not included in the analysis. As shown previously for benzene [32], the higher-resolution cryobeam will be necessary to resolve these features and obtain a more precise measurement of ε_b.

Shown in Fig. 4(c) is the measured annihilation spectrum for pyridine. Pyridine has a benzenelike structure with a C-H group replaced by a nitrogen. Like benzene, it has three π bonds. Due to the substitution, it has a dipole moment of 2.19 D. The spectrum has a single prominent peak at $E_\parallel \approx 0.19$ eV which is associated with the phenyl C-H stretch modes. The result is $\varepsilon_b = 186 \pm 5$ meV. Although the peak is well resolved, like that in benzene, there is a broad, relatively flat region of enhanced annihilation at energies below the C-H stretch peak extending to the low-energy limit of the measurements. This is likely due to multimode VFRs. Surprisingly, the IR spectrum does not show significant IR activity over much of this
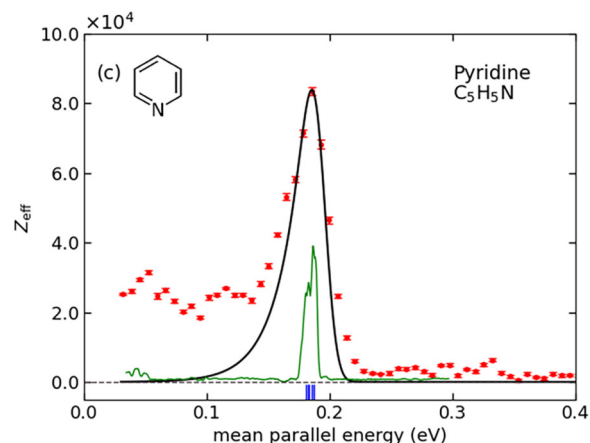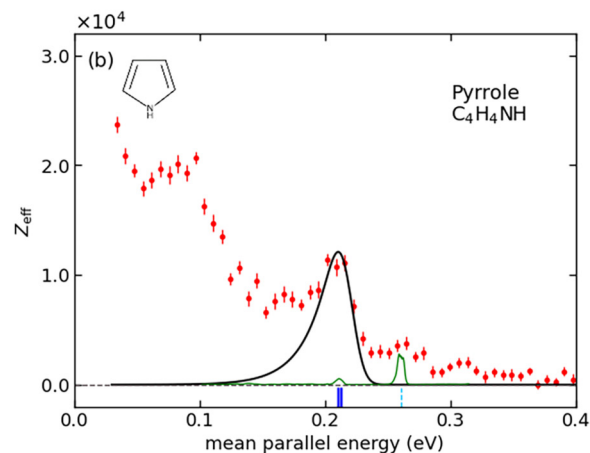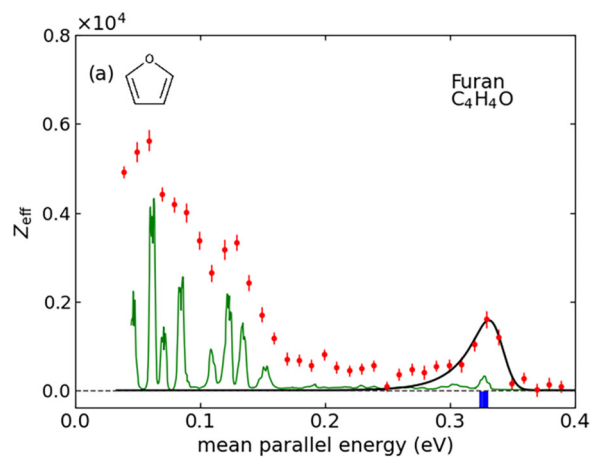

FIG. 4. Z_{eff} measurements for (a) furan, (b) pyrrole, and (c) pyridine. The green curves are the infrared (IR) spectra obtained from NIST [37], and vertical blue bars indicate the locations of the IR-active fundamental modes, with both downshifted by ε_b. The solid black curves are fits to the C-H stretch peaks. Vertical light blue dashed lines indicate dipole-active modes not used in the analysis.

region. Understanding these features is a topic of current research.

Pyridazine adds a second nitrogen to the pyridine structure and thus is a diazine. In this case, the dipole moment almost doubles to 4.2 D, and so it is expected to have a significantly higher ε_b value than pyridine. The measured annihilation
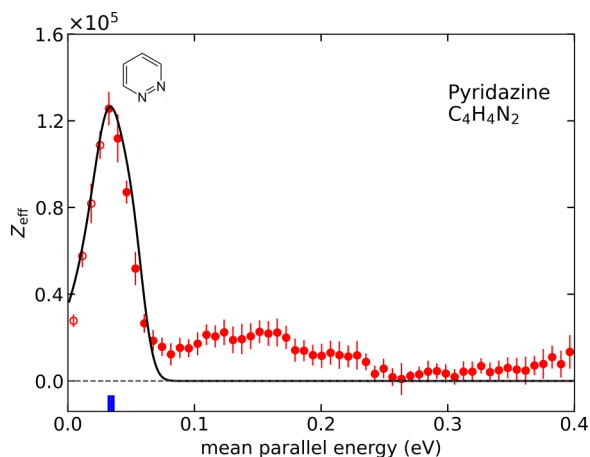
FIG. 5. Z_{eff} measurements for pyridazine. The vertical blue bars indicate the locations of the infrared (IR)-active fundamental modes, with both downshifted by ε_b. The solid black curves are fits to the C-H stretch peaks. Hollow circles are data where systematic errors cannot be ruled out (see text for details).

spectrum is shown in Fig. 5. The spectrum shows an apparent peak at $E_\parallel \approx 0.04$ eV, which is at the low-energy limit of our measurements. To resolve the peak position, the data must be extended down to near $E_\parallel \approx 0$. Due to nonideal effects, including approaching the beam cutoff and scattering effects at low energies, neither the magnitude of the peak nor the position is assured to be reliable. Neglecting this consideration and ascribing the peak to the four phenyl CH mode yields $\varepsilon_b = 330$ meV. Assuming the mode identification is correct, we can use the fit to the high-energy side of the peak to state that $\varepsilon_b \geqslant 330$ meV (i.e., a lower bound on ε_b). Above the main peak, there is a broad range of enhanced annihilation extending to ~0.25 eV. This feature is like that seen in benzene and several deuterated benzenes [32]. It is also prominent in many other aromatics (e.g., phenylacetylene [Fig. 2(e)]), and is an important topic for future study.

C. Nonaromatic cyclic molecules

All of the molecules discussed above were aromatics. This raises the question as to whether or how aromaticity affects ε_b. In a previous study, we measured ε_b for several five and six carbon alkane rings at different levels of saturation [15], all of which had zero or very small dipole moments ($\mu < 0.5$). Those molecules exhibited modest increases of ε_b with increasing N_π, but they each had only one or two π bonds. To extend the comparison to nonaromatic molecules with larger N_π, we measured the spectra for CHT (C_7H_8, 3 π bonds), and COT (C_8H_8, 4 π bonds). The results and comparison with the analogous saturated seven and eight carbon alkanes are included in Table I.

Spectra for CHT and COT are shown in Figs. 6(a) and 6(b). In the case of CHT, a VFR peak is observed at $\simeq 0.17$ eV, dominated by the C-H stretch vibrational modes. Here, the peak is broadened because there are two types of C-H stretch modes with different characteristic energies. Using all eight modes, we obtain $\varepsilon_b = 190 \pm 8$ meV. The curve fits reasonably well, but there appears to be extra spectral weight that is not accounted for on both sides of the peak. Further, the model assumed equal amplitude for all eight modes. If that is incorrect, it could shift the measured ε_b value by several meV, leading to a larger uncertainty for this molecule.

For COT, there are six distinct C-H stretch modes (two degenerate) with three non-dipole-active modes. Using only the dipole-active modes, $\varepsilon_b = 225 \pm 5$ meV. There also appears to be some broadening on the low-energy side of the peak, but in contrast with CHT, the peak is well fit. Thus, this broadening does not appear to significantly affect ε_b. For both molecules (more so COT), there is a broad region of enhanced annihilation above the CH resonance. This is very similar to what was seen in the aromatics discussed above. While not presently understood, it appears that this extra structure is most prominent in molecules with appreciable symmetry.

With regard to the ε_b values, although COT has no dipole moment, the presence of the extra π bond and more symmetric structure of the molecule leads to a larger binding energy (i.e., a difference of >35 meV) compared with CHT. We can also compare the binding energies of these molecules with the
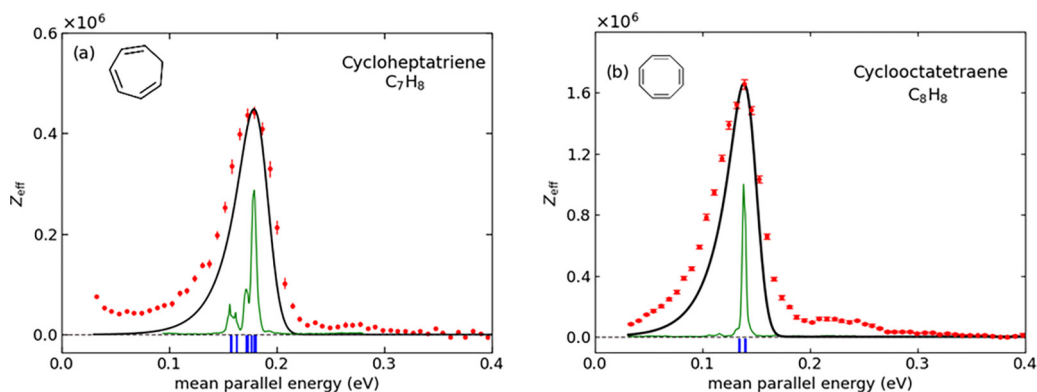

FIG. 6. Z_{eff} measurements for the nonaromatic and ring molecules (a) cycloheptatriene and (b) cyclooctatetraene. The green curves are the infrared (IR) spectra obtained from NIST [37], and vertical blue bars indicate the locations of the IR-active fundamental modes, with both downshifted by ε_b. The solid black curves are fits to the C-H stretch peaks.

saturated rings cycloheptane and cyclooctane, Ref. [12]. For CHT as compared with cycloheptane, adding three π bonds increases ε_b by $\sim$80 meV. For COT compared with cyclooctane, a larger increase of $\sim$100 meV is observed by adding the four π bonds. This trend extends the results observed for the smaller rings [12] to larger numbers of π bonds and shows the strong impact that N_π has on ε_b.

IV. THEORY OF POSITRON BINDING AND COMPARISONS WITH EXPERIMENTAL MEASUREMENTS

Positron binding energies are calculated here for the molecules considered via *ab initio* many-body theory [27], assuming fixed nuclei [49]. The approach is implemented in the EXCITON+ code, which is heavily adapted from the original EXCITON all-electron molecular many-body code [50] to include positrons. The positron binding energies are found by solving the Dyson equation [51,52]:

$$(H^{(0)} + \hat{\Sigma}_\varepsilon)\psi_\varepsilon(\mathbf{r}) = \varepsilon\psi_\varepsilon(\mathbf{r}), \tag{3}$$

where $\psi_\varepsilon(\mathbf{r})$ is the quasiparticle positron wave function with energy ε, $H^{(0)}$ is the Hamiltonian of the positron in the static (Hartree-Fock) field of the ground-state molecule, and $\hat{\Sigma}_\varepsilon$ is the energy-dependent correlation potential (self-energy of the positron in the field of the molecule) that accounts for electron-positron correlations. The energy dependence of Σ demands a self-consistent solution of Eq. (3) for the bound state with $\varepsilon_b = |\varepsilon|$ for negative eigenvalues ε. The approach includes three main diagrammatic contributions to the positron-molecule self-energy (see fig. 1 of Ref. [27]). The first is the *GW* contribution, Σ^{GW}, which accounts for polarization of the molecular electron cloud by the positron, screening of the electron-positron Coulomb interaction (the random phase approximation (RPA) ring series), and electron-hole attraction (time-dependent-Hartree-Fock or Bethe-Salpeter-equation (BSE) approximation, depending on whether bare or screened electron-hole Coulomb interactions are used within the ring series). The second contribution describes the nonperturbative process of virtual-positronium formation (where a molecular electron temporarily tunnels to the positron, leading to an attractive interaction), via calculation of the infinite ladder series of electron-positron interactions Σ^Γ. The third contribution is an analogous diagram containing the ladder series for positron-hole repulsion, Σ^Λ. We calculate the total self-energy via their sum as $\Sigma = \Sigma^{GW} + \Sigma^\Gamma + \Sigma^\Lambda$.

The positron and electron wave functions are expanded in distinct Gaussian basis sets, centered at each atom in the molecule and at 5–10 additional ghost centers $\sim$1 Å from the molecule. This combination enables a good description of the positron wave function at the nuclei and in the regions close to the molecule where virtual-positronium formation occurs (see Ref. [27] for more details). For both the electron and positron bases, diffuse-function-augmented correlation-consistent polarized aug-cc-pVXZ (X = T, Q) Dunning basis sets [53] are employed. An additional large even-tempered basis set is included for the positron at the region of highest positron density, or at the center of the molecule, to account for long-range correlations. The even-

tempered bases have exponents $\zeta_k = \zeta_0\beta^{k-1}$, $k = 1, 2, \ldots$ and take the form $10s\,9p\,8d\,7f\,3g$ with $\beta = 2.2$, $\zeta_0 = 10^{-3}$ for all molecules except COT, benzene, and phenylacetylene, which have $10s\,9p\,8d\,7f\,6g$ with $\beta = 2.0$ and $\zeta_0 = 10^{-3}$ (benzene and phenylacetylene) or $\zeta_0 = 10^{-4}$ (COT). Solution of the Dyson equation for the molecules considered required diagonalization of Casida matrices of size $0.5M \times 0.5M$, requiring $\sim$15 TB RAM. They were performed on the UK Tier-2 HPC cluster Kelvin2 and the UK National Supercomputer ARCHER2.

The calculated binding energies are presented in Table II at three successively more sophisticated levels of MBT which differ in the approximation used to calculate the ladder series for the virtual positronium formation and positron-hole repulsion self-energy contributions: the first (second) uses bare (screened) Coulomb interactions in the ladder diagrams and Hartree-Fock molecular orbital energies, and the third, the most sophisticated approach, uses screened Coulomb interactions and molecular orbital energies calculated at *GW* level [50,54].

Additionally, results are shown for a model approach [27], which approximates the computationally expensive virtual-positronium formation self-energy Σ^Γ by scaling the bare polarization self-energy $\Sigma^{(2)}$ by a factor g so that $\Sigma \approx g\Sigma^{(2)} + \Sigma^\Lambda$. In the molecules studied to date [19,27] and here, setting $g = 1.4$ and 1.5 provides good lower and upper bounds for the positron binding energy, respectively. Table II also contains calculated values of the dipole moment μ, dipole polarizability α, and ionization energy I, which are in good agreement with the reference values in Table I.

Comparison of the predicted and measured binding energies is shown in Fig. 7. Agreement is good to excellent. For the 11 molecules for which ε_b is given in Table II, the root mean square (rms) difference in binding energy between theory (using values in bold) and experiment is 18 meV. This corresponds to an rms fractional deviation in the experimental and calculated binding energies $[\varepsilon_b(\text{calc.}) - \varepsilon_b(\text{exp.})]/\varepsilon_b(\text{exp.})$ of 10%. One noticeable trend is that, of the comparisons presented here, the measured binding energies of 6 of the 11 molecules are larger than the theoretical prediction, three are within the experimental error bars, and only two measured values (benzene and benzonitrile) are smaller than that predicted.

Finally, having the positron bound-state wave function enables calculation of the electron-positron annihilation contact density δ as
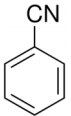
$$\delta = \sum_{n=1}^{N_e} \gamma_n \int |\phi_n(\mathbf{r})|^2 |\psi_\varepsilon(\mathbf{r})|^2 d\mathbf{r}, \tag{4}$$

where $\phi_n(\mathbf{r})$ are the occupied electronic molecular orbitals, the sum is over the N_e occupied electron orbitals, and γ_n are enhancement factors which account for short-range electron-positron attraction and depend on the *GW* ionization energy ε_n of each molecular orbital as follows [55]: $\gamma_n = 1 + \sqrt{1.31/|\varepsilon_n|} + (0.834/|\varepsilon_n|)^{2.15}$.
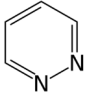
TABLE II. Calculated MBT positron binding energies ε_b (meV) for ringed molecules compared with experiment (ordered by successively decreasing dipole moment). Also shown are dipole moments μ (calculated at HF), dipole polarizabilities α (calculated at the $GW@BSE$ level of MBT), ionization energies I (calculated at HF and the $GW@RPA$ level of MBT), and annihilation contact densities (calculated at the $GW + \Gamma + \Lambda$ level of MBT with enhancement factors [55]).

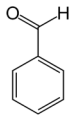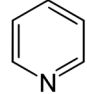|		Molecular properties			Positron binding energy (meV)			
Molecule	Formula	μ (D)	α (Å^3)	I (eV)[a]	MBT[b]	Exp.[c]	MBT model[d]	δ (a.u.)[e]
Benzonitrile	C_6H_5CN	4.9	12.1	9.86, 10.07	326, 303, **331**	298 ± 5	284, 343	1.60[−2]
Pyridazine	$C_4H_4N_2$	4.3	8.2	10.57, 10.87	334, 308, **333**	330 ± 10	327, 398	1.89[−2]
Benzaldehyde	C_6H_5CHO	3.5	11.9	9.64, 9.90	210, 192, **213**	220 ± 10	198, 256	1.46[−2]
Pyridine	C_5H_5N	2.3	8.9	9.52, 9.91	184, 155, **181**	186 ± 5	149, 211	1.58[−2]
Pyrrole	C_4H_4NH	1.9	7.6	8.22, 8.64	157, 127, **148**	165 ± 10	94, 148	1.55[−2]
Aniline	$C_6H_5NH_2$	1.4	11.0	8.07, 8.26	220, 180, **209**	233 ± 5	172, 251	1.92[−2]
Phenylacetylene	C_6H_5CCH	0.8	13.3	8.86, 9.15	229, 187, **220**	230 ± 5	183, 266	1.87[−2]
Furan	C_4H_4O	0.7	6.7	8.85, 9.35	45, 32, **42**	52 ± 5	20, 49	7.32[−3]
Toluene	$C_6H_5CH_3$	0.4	11.4	8.87, 9.14	174, 135, **161**	173 ± 5	128, 203	1.87[−2]
Benzene	C_6H_6	0.0	9.8	9.21, 9.57	158, 122, **148**	132 ± 3	96, 160	1.61[−2]
COT	C_8H_8[f]	0.0	13.0	8.37, 8.66	202, 158, **190**	225 ± 5	151, 238	2.03[−2]

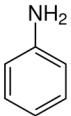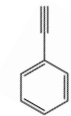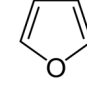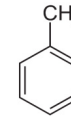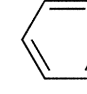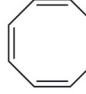| Benzonitrile | Pyridazine | Benzaldehyde | Pyridine | Pyrrole | Aniline | Phenylacetylene | Furan | Toluene | Benzene | Cyclooctatetraene |
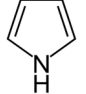
[a]The first (second) number is that calculated at HF ($GW@RPA$).
[b]Many-body calculations at three levels of $\Sigma^{GW+\Gamma+\Lambda}$: (i) using bare Coulomb interactions within the ladders and HF energies; (ii) using dressed Coulomb interactions within the ladders and HF energies; and (iii) using dressed Coulomb interactions and $GW@RPA$ energies. The latter (highlighted in bold) is the most sophisticated calculation.
[c]This paper, see Table I.
[d]Using a scaled self-energy to account for virtual positronium formation [27], $\Sigma \approx g\Sigma^{(2)} + \Sigma^\Lambda$, with $g = 1.4$ and 1.5.
[e]Figures in square brackets indicate powers of 10.
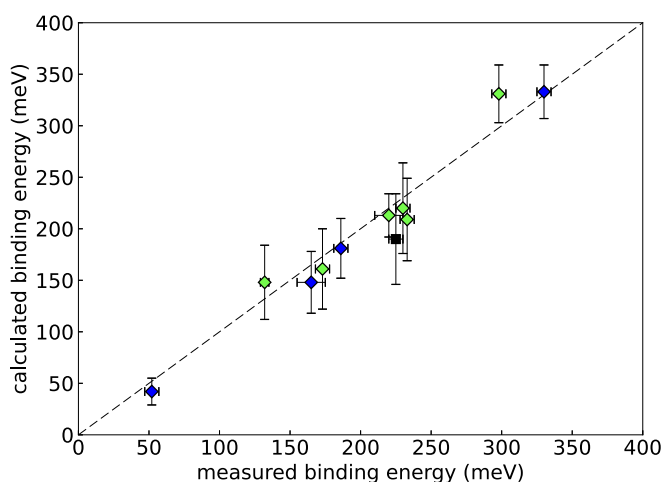[f]In the 'tub' (D_{2d}) geometry.

FIG. 7. Comparison of the calculated binding energies vs the measured binding energies. Green diamonds: benzene and benzene substitutions; blue diamonds: heterocyclic aromatic molecules; black square: COT. Error bars on the calculated values are the maximum difference between results from the three many-body calculations in Table II.

V. FURTHER DISCUSSION

A. Localization of the bound-state positron wave function

The bound-state positron wave functions for the molecules studied here are shown in Fig. 8. With one exception [Fig. 8(f), right], they show the 80% maximum isosurface. This highlights regions of relatively strong localization. Lower amplitude isosurfaces are more delocalized (e.g., panel (f), right, and Fig. 9 as discussed below). For molecules where the aromatic π bonds dominate, the positron wave function is localized in planes above and below the plane of the molecule where the π-bond electron density is largest. Examples of this effect are seen in Figs. 8(j) and 8(i), benzene and toluene, respectively. In contrast, like what was seen with nonaromatic molecules [27], the calculations show that the introduction of a large permanent dipole moment results in localization of the wave function very near the dipole, as seen in Figs. 8(c), 8(b), and 8(d) for benzaldehyde, pyridazine, and pyridine, respectively.

However, the effects of attraction of the positron to the π-bond electrons and to a permanent dipole compete when both are present on the same molecule. As examples, aromatic π-bond localization is seen to be (weakly) perturbed by the dipoles in Figs. 8(f) and 8(e), aniline and pyrrole, respectively. A stronger effect is seen in (h) furan, where the 80% positron contour extends from the region of the π-bond electrons all the way to the dipole. The C≡C triple-bond π orbitals in (g)
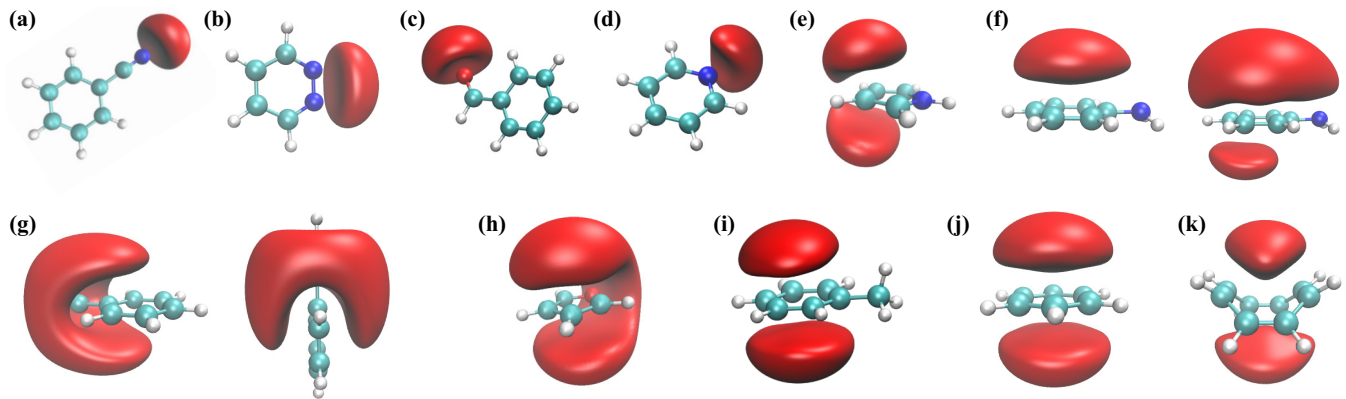
FIG. 8. Correlated positron Dyson wave functions (positive and real as displayed here) for several heterocyclic molecules at the $GW + \Gamma + \Lambda$ level of many-body theory, shown at 80% of the wave function maximum unless otherwise stated, and ordered by successively decreasing dipole moment. (a) Benzonitrile, (b) pyridazine, (c) benzaldehyde, (d) pyridine, (e) pyrrole, (f) aniline (left, 80%; right, 60%), (g) phenylacetylene (two orientations, both 80%), (h) furan, (i) toluene, (j) benzene, and (k) cyclooctatetraene (D_{2d} geometry).

phenylacetylene result in concentration of the positron around this bond, which extends continuously into the region of the aromatic π-bond electrons. Changes in molecular symmetry can also affect π-bond localization. An example of this is the distorted positron wave function contour resulting from the broken planar symmetry of cyclooctatetraene. Figure 8(f) for aniline shows that the strong, slightly-out-of-plane dipole results in restricting the 80% positron wave function contour

to the region above the plane, whereas the 65% contour shows some amplitude below the plane as well.

To see the structure in more detail, Fig. 9 shows contours of the positron wave function for pyridazine, phenylacetylene, and aniline in the plane of the ring and in a plane perpendicular to the ring. As expected, there is little or no amplitude near the atomic cores. The figure shows delocalized areas of the positron wave function around the molecule (to distances of $\sim$10 a.u.) and also the regions of larger amplitude shown in
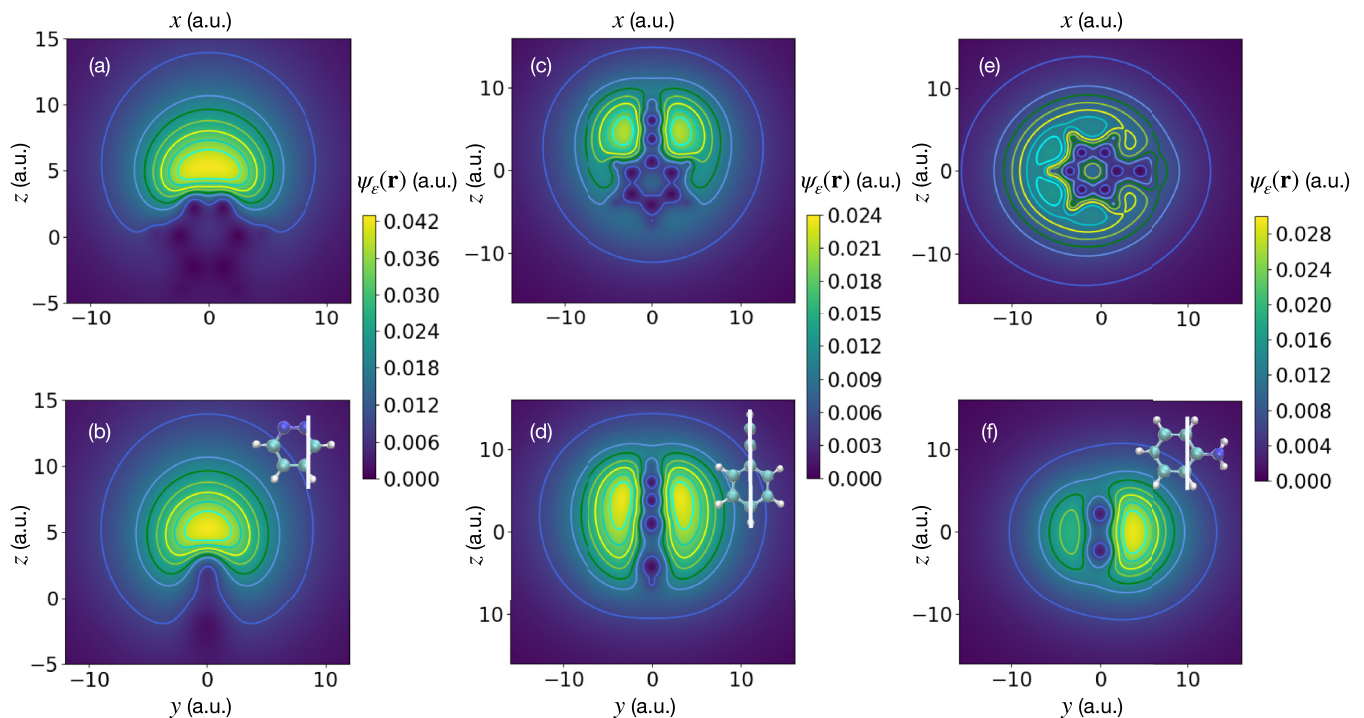

FIG. 9. The positron Dyson wave functions $\psi_\varepsilon(\mathbf{r})$ calculated at the $GW + \Gamma + \Lambda$ level of many-body theory: (a) Pyridazine in a plane containing the ring; (b) pyridazine in a plane perpendicular to the ring (see inset image); (c) phenylacetylene (PA) in a plane containing the ring; (d) phenylacetylene in a plane perpendicular to the ring and containing the CCH group (see inset image); (e) aniline in a plane containing the ring; and (f) aniline in a plane perpendicular to the ring (see inset image). Contours are shown at 90, 80, 70, 60, 50, 40, and 20% of the wave function maximum value in each plane considered. For each molecule, the maximum color bar value is the maximum value of the wave function attained over both planes considered. These maxima all coincided with the global wave function maxima for each molecule considered, specifically 0.042 a.u. for pyridazine, 0.024 a.u. for phenylacetylene, and 0.029 a.u. for aniline.
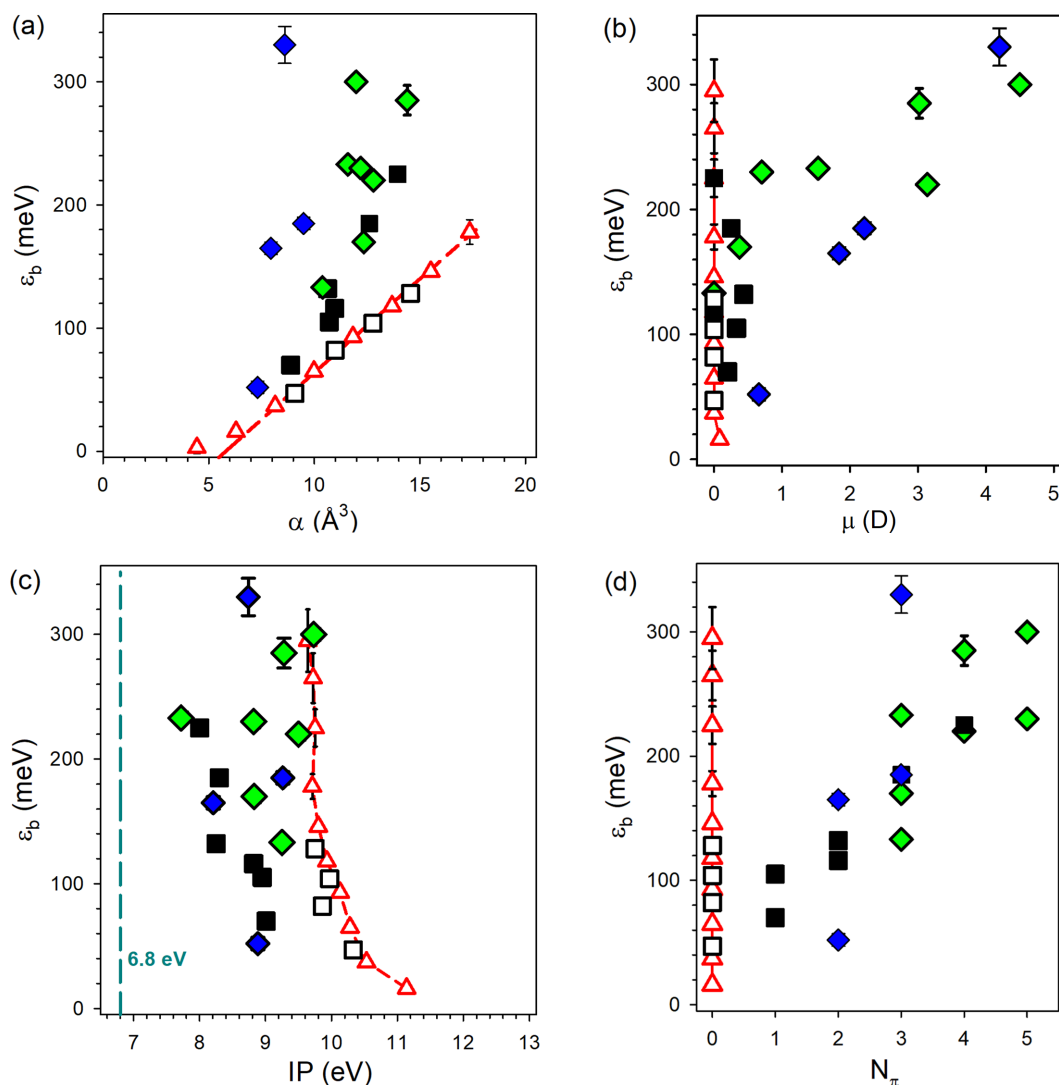
FIG. 10. Measurements of ε_b for aromatic and ring molecules vs (a) molecular polarizability α, (b) permanent dipole moment μ, (c) ionization potential I, and (d) number of π bonds N_π. Diamonds: Six-member carbon aromatic rings: green, benzene and benzene substitutions; blue, heterocyclic molecules. Squares: Five-member nonsaturated and nonaromatic carbon rings. Red triangles: Alkanes. Black symbols: Cyclic molecules. Solid symbols: One or more π bonds. Open symbols: no π bonds. Data for alkanes from Ref. [12] and other nonsaturated rings from Ref. [15].

Fig. 8 due to attraction to the negative ends of the dipoles and to regions of π-bond electrons.

B. Relationship of ε_b to molecular parameters

It has been natural to try to relate binding energies to global molecular parameters such as α, μ, I, and N_π, and much has been written on this topic. It has also been shown by comparison of isomers that molecular geometry can play an important role in positron binding, irrespective of other global parameters [20,56]. Shown in Fig. 10 are ε_b values for the molecules studied here and selected previous data as a function of α, μ, I, and N_π, extending the ranges of parameters studied beyond those done previously.

There is naturally a large scatter in the data in the one-parameter-at-a-time representations in Fig. 10 since wide

variations of the other parameters (not shown in a particular plot) produce changes in ε_b as well. Despite the large scatter in the data, it is apparent that there are changes in ε_b associated with changes in μ and N_π [cf. panels (b) and (d)]. This highlights the role of μ and N_π in determining ε_b for the molecules studied here, like that seen in the spatial distribution of the positron wave function.

From the data in Fig. 10(c), ε_b appears to be independent of I, to within the scatter in the values. This is made clearer when one separately considers I for aromatic and nonaromatic rings. They span narrower bands of I at differing mean I (i.e., separated by ~ 0.8 eV) but exhibit similar broad ranges of ε_b. This tends to confirm that ε_b depends only weakly, if at all, on I for the molecules studied here.

Regarding the dependence of ε_b on N_π, the molecules shown in Fig. 10 include different types of π bonds: aromatic

and nonaromatic π bonds in rings, π orbitals in C=O double bonds, and π bonds in the C≡C triple bond in phenylacetylene. When all are included [cf. Fig. 10(d)], they indicate that ε_b increases with increasing N_π. While these limited data constrain detailed analysis, it also appears that the change in ε_b with N_π is similar for the aromatic and nonaromatic π bonds. Thus, the present data are consistent with all π bonds contributing approximately equally to ε_b, but more precise conclusions will require further study.

C. Multimode phenomena in ring molecules

A theory of coupling to dipole-allowed transitions is successful in explaining VFR due to fundamental modes in small molecules [30], and there were two observations of similar quadrupole coupling [31]. Going further, it is natural to try to associate annihilation VFR not associated with dipole- and quadrupole-allowed fundamental vibrations with other IR activity in the molecule. However, a detailed explanation is lacking of many of the observed regions of enhanced annihilation that do not appear to correspond to fundamental vibrational modes. The working assumption is that these resonances are due to as yet unidentified multimode resonances (e.g., combinations and overtones), but this has yet to be confirmed. The special case of the FR in benzaldehyde offers an opportunity to study such multimode resonances, for a case in which the individual modes have been identified. Better positron beam resolution will be needed to study this FR in further detail.

There are also regions in the annihilation spectra where broad VFR activity is observed that does not appear to correspond to appreciable IR activity. Examples presented here are the spectra of benzene, pyridine, and pyrrole. This raises the question as to whether there is some other, presently unrecognized, annihilation VFR mechanism (i.e., not visible in IR spectral measurements), but this is beyond the scope of this paper.

VI. SUMMARY AND CONCLUDING REMARKS

There has been much progress in understanding positron binding to molecules (e.g., Refs. [2,3,13,16–19,27,30,57,58]), but many questions remain. In this paper, we have presented a study of resonant positron annihilation and positron binding in selected aromatic and ring compounds. It enabled an investigation of the effects of permanent dipole moment and π orbitals, and the competition of the two, in determining positron annihilation and binding. Experimental measurements for ε_b were compared with the predictions of a recent *ab initio* MBT. Good to excellent agreement was found (i.e., 10% rms fractional deviation between measurements and predictions for 11 molecules). This is made more significant by the fact that the compounds span a wide range of N_π (2–5), μ (0.3–4.5 D), and a factor of 1.7 in α.

An important result of the theory is predictions for the spatial distribution of the bound positron wave function. This can be used to distinguish the different character of the bound states due to specific molecular parameters. As established

previously, the polarizability results in a more or less uniform bound-state density surrounding the molecule, while a permanent dipole moment localizes the bound-state density near the dipole. Aromatic π bonds produce maxima in positron density above and below the planes of the ring molecules. A related π-bond localization effect is seen in the nonvalence anion $C_6F_6^-$ in which the excess (weakly bound) electron has a very similar charge distribution to that of a positron attached to benzene, C_6H_6 [59,60].

This qualitative picture of positron wave function localization provides insight into positron-molecule bound states complementary to the quantitative predictions of the theory. An interesting question for future study is whether one could distinguish experimentally the π and μ components of the bound state wave function using γ-ray spectroscopy [i.e., Doppler-broadening or angular correlation of annihilation radiation (ACAR)] [61].

The observed enhancements in Z_{eff} are much larger than those predicted by the simple GL theory [30], and this represents a major gap in our understanding. One example of the chemical specificity discussed here is the increase in Z_{eff} by a factor of 30 when a methyl group is added to benzene. Similarly, some modes, such as the methyl/phenyl C-H modes, are enhanced while others, such as the acetyleneic C-H, N-H and O-H modes in alcohols, are not. These modes have significant IR amplitudes (sometimes larger than the methyl C-H stretch modes) but no obvious enhancement.

Another example of chemical specificity is the large amount of likely multimode spectral weight at low energies in pyrrole, relative to that due to the C-H stretch mode. That the observed annihilation VFR can be smaller or orders of magnitude larger than the predictions of simple theory has been attributed to vibrational coupling to other modes (i.e., IVR) [2]; however, attempts to pursue this have, as yet, had only modest success [33]. Similarly, there is now appreciable evidence of multimode annihilation VFR (e.g., in benzene, benzaldehyde, and furan) but little understanding of when and how this occurs. The observation of the annihilation FR in benzaldehyde may provide further insight into this phenomenon.

[1] C. M. Surko, A. Passner, M. Leventhal, and F. J. Wysocki, Bound states of positrons and large molecules, Phys. Rev. Lett. **61**, 1831 (1988).

[2] G. F. Gribakin, J. A. Young, and C. M. Surko, Positron-molecule interactions: Resonant attachment, annihilation, and bound states, Rev. Mod. Phys. **82**, 2557 (2010).

[3] G. F. Gribakin and C. M. R. Lee, Positron annihilation in large polyatomic molecules, Eur. Phys. J. D **51**, 51 (2009).

[4] V. A. Dzuba, V. V. Flambaum, G. F. Gribakin, and W. A. King, Bound states of positrons and neutral atoms, Phys. Rev. A **52**, 4541 (1995).

[5] G. G. Ryzhikh and J. Mitroy, Positronic lithium, an electronically stable Li-e$^+$ ground state, Phys. Rev. Lett. **79**, 4124 (1997).

[6] K. Strasburger and H. Chojnacki, Quantum chemical study of simple positronic systems using explicitly correlated Gaussian functions—PsH and PsLi$^+$, J. Chem. Phys. **108**, 3218 (1998).

[7] J. Mitroy and G. G. Ryzhikh, Measuring the positron affinities of atoms, J. Phys. B **32**, L411 (1999).

[8] V. A. Dzuba, V. V. Flambaum, and G. F. Gribakin, Detecting positron-atom bound states through resonant annihilation, Phys. Rev. Lett. **105**, 203401 (2010).

[9] C. M. Surko, J. R. Danielson, G. F. Gribakin, and R. E. Continetti, Measuring positron–atom binding energies through laser-assisted photorecombination, New J. Phys. **14**, 065004 (2012).

[10] A. R. Swann, D. B. Cassidy, A. Deller, and G. F. Gribakin, Formation of positron-atom bound states in collisions between Rydberg Ps and neutral atoms, Phys. Rev. A **93**, 052712 (2016).

[11] J. R. Danielson, J. A. Young, and C. M. Surko, Dependence of positron-molecule binding energies on molecular properties, J. Phys. B: At. Mol. Opt. Phys. **42**, 235203 (2009).

[12] J. R. Danielson, S. Ghosh, E. Arthur-Baidoo, D. R. Witteman, and C. M. Surko, Positron binding to alkane molecules, Phys. Rev. A **108**, 032801 (2023).

[13] A. R. Swann, G. F. Gribakin, J. R. Danielson, S. Ghosh, M. R. Natisin, and C. M. Surko, Effect of chlorination on positron binding to hydrocarbons: Experiment and theory, Phys. Rev. A **104**, 012813 (2021).

[14] J. R. Danielson, A. C. L. Jones, J. J. Gosselin, M. R. Natisin, and C. M. Surko, Interplay between permanent dipole moments and polarizability in positron-molecule binding, Phys. Rev. A **85**, 022709 (2012).

[15] J. R. Danielson, S. Ghosh, and C. M. Surko, Enhancement of positron binding energy in molecules containing π bonds, Phys. Rev. A **106**, 032811 (2022).

[16] A. R. Swann and G. F. Gribakin, Positron binding and annihilation in alkane molecules, Phys. Rev. Lett. **123**, 113402 (2019).

[17] Y. Sugiura, T. Takayanagi, and M. Tachikawa, Theoretical calculation of positron annihilation spectrum using positron-electron correlation-polarization potential, Int. J. Quantum Chem. **120**, e26376 (2020).

[18] Y. Sugiura, H. Suzuki, T. Otomo, T. Miyazaki, T. Takayanagi, and M. Tachikawa, Positron–electron correlation-polarization potential model for positron binding in polyatomic molecules, J. Comput. Chem. **41**, 1576 (2020).

[19] J. P. Cassidy, J. Hofierka, B. Cunningham, C. M. Rawlins, C. H. Patterson, and D. G. Green, Many-body theory calculations of positron binding to halogenated hydrocarbons, Phys. Rev. A **109**, L040801 (2024).

[20] A. Swann and G. Gribakin, Effect of molecular constitution and conformation on positron binding and annihilation in alkanes, J. Chem. Phys. **153**, 184311 (2020).

[21] S. d'A. Sanchez, M. A. P. Lima, and M. T. do N. Varella, Multimode vibrational couplings in resonant positron annihilation, Phys. Rev. Lett. **107**, 103201 (2011).

[22] A. S. Barbosa, F. Blanco, G. García, and M. H. Bettega, Theoretical study on positron scattering by benzene over a broad energy range, Phys. Rev. A **100**, 042705 (2019).

[23] G. M. Moreira and M. H. Bettega, Elastic scattering of slow positrons by pyrazine, J. Phys. Chem. A **123**, 9132 (2019).

[24] D. Edwards, D. Stevens, Z. Cheong, V. Graves, J. Gorfinkiel, F. Blanco, G. Garcia, M. Brunger, R. White, and J. Sullivan, Positron scattering from pyrazine, Phys. Rev. A **104**, 042807 (2021).

[25] V. Graves and J. D. Gorfinkiel, R-matrix calculations for elastic electron and positron scattering from pyrazine: Effect of the polarization description, Eur. Phys. J. D **76**, 43 (2022).

[26] G. M. Moreira and M. H. Bettega, Can a positron bind to the para-benzoquinone molecule? Eur. Phys. J. D **78**, 9 (2024).

[27] J. Hofierka, B. Cunningham, C. M. Rawlins, C. H. Patterson, and D. G. Green, Many-body theory of positron binding to polyatomic molecules, Nature (London) **606**, 688 (2022).

[28] C. M. Rawlins, J. Hofierka, B. Cunningham, C. H. Patterson, and D. G. Green, Many-body theory calculations of positron scattering and annihilation in H_2, N_2, and CH_4, Phys. Rev. Lett. **130**, 263001 (2023).

[29] J. P. Cassidy, J. Hofierka, B. Cunningham, and D. G. Green, Many-body theory calculations of positronic-bonded molecular dianions, J. Chem. Phys. **160**, 084304 (2024).

[30] G. F. Gribakin and C. M. R. Lee, Positron annihilation in molecules by capture into vibrational Feshbach resonances of infrared-active modes, Phys. Rev. Lett. **97**, 193201 (2006).

[31] M. R. Natisin, J. R. Danielson, G. F. Gribakin, A. R. Swann, and C. M. Surko, Vibrational Feshbach resonances mediated by nondipole positron-molecule interactions, Phys. Rev. Lett. **119**, 113402 (2017).

[32] S. Ghosh, J. R. Danielson, and C. M. Surko, Resonant annihilation and positron bound states in benzene, Phys. Rev. Lett. **129**, 123401 (2022).

[33] G. F. Gribakin, J. F. Stanton, J. R. Danielson, M. R. Natisin, and C. M. Surko, Mode coupling and multiquantum vibrational excitations in Feshbach-resonant positron annihilation in molecules, Phys. Rev. A **96**, 062709 (2017).

[34] R. Iida, H. Suzuki, T. Takayanagi, and M. Tachikawa, Contribution of vibrational overtone excitations to positron annihilation rates for benzene and naphthalene, Phys. Rev. A **104**, 062807 (2021).

[35] M. R. Natisin, J. R. Danielson, and C. M. Surko, Formation of buffer gas trap-based positron beams, Phys. Plasmas **22**, 033501 (2015).

[36] S. Ghosh, J. Danielson, and C. Surko, Energy distribution and adiabatic guiding of a solid-neon-moderated positron beam, J. Phys. B: At. Mol. Opt. Phys. **53**, 085701 (2020).

[37] P. Linstorm and W. G. Mallard (eds.), *NIST Chemistry Web-Book, NIST Standard Reference Database Number 69* (National Institute of Standards and Technology, Gaithersburg, 2023).

[38] G. Gribakin and P. Gill, The role of vibrational doorway states in positron annihilation with large molecules, Nucl. Instrum. Methods Phys. Res. B **221**, 30 (2004).

[39] G. M. Stewart and J. D. McDonald, Intramolecular vibrational relaxation from C-H stretch fundamentals, J. Chem. Phys. **78**, 3907 (1983).

[40] W. M. Haynes, *CRC Handbook of Chemistry and Physics* (CRC Press, Boca Raton, 2016).

[41] R. D. Johnson III (ed.), NIST Computational Chemistry Comparison and Benchmark Database, NIST Standard Reference Database Number 101, Release 16a, http://cccbdb.nist.gov/ (accessed Mar 13, 2015).

[42] N. Fuson, C. Garrigou-Lagrange, and M. Josien, Spectre infrarouge et attribution des vibrations des toluènes $C_6H_5CH_8$, $C_6H_5CD_8$ et $C_6D_5CD_3$, Spectrochim. Acta **16**, 106 (1960).

[43] A. Gambi, S. Giorgianni, A. Passerini, R. Visinoni, and S. Ghersetti, Infrared studies of acetophenone and its deuterated derivatives, Spectrochim. Acta A-M **36**, 871 (1980).

[44] O. Desyatnyk, L. Pszczółkowski, S. Thorwirth, T. Krygowski, and Z. Kisiel, The rotational spectra, electric dipole moments and molecular structures of anisole and benzaldehyde, Phys. Chem. Chem. Phys. **7**, 1708 (2005).

[45] J. H. S. Green and D. J. Harrison, Vibrational spectra of benzene derivatives—XVI. Benzaldehyde and mono-substituted benzaldehydes, Spectrochim. Acta A-M **32**, 1265 (1976).

[46] G. Tolstorozhev, I. Skornyakov, M. Bel'kov, O. Shadyro, S. Brinkevich, and S. Samovich, IR spectra of benzaldehyde and its derivatives in different aggregate states, Opt. Spectrosc. **113**, 179 (2012).

[47] A. Mellouki, J. Liévin, and M. Herman, The vibrational spectrum of pyrrole (C_4H_5N) and furan (C_4H_4O) in the gas phase, Chem. Phys. **271**, 239 (2001).

[48] A. C. L. Jones, J. R. Danielson, J. J. Gosselin, M. R. Natisin, and C. M. Surko, Positron binding to alcohols, New J. Phys. **14**, 015006 (2012).

[49] Note that vibrational and geometry relaxation effects are known to typically provide a few percent correction to fixed-nuclei calculations of binding energies and wave function densities [2,58,62–65]. Further, resonant annihilation studies of deuterated molecules have shown that there is no change in the binding energies upon the substitution H → D, suggesting that positron binding energies are weakly affected by vibrations [2,32].

[50] C. H. Patterson, Photoabsorption spectra of small Na clusters: TDHF and BSE versus CI and experiment, Phys. Rev. Mater. **3**, 043804 (2019).

[51] A. L. Fetter and J. D. Walecka, *Quantum Theory of Many-Particle Systems* (Dover, New York, 2003).

[52] W. H. Dickhoff and D. V. Neck, *Many-Body Theory Exposed!—Propagator Description of Quantum Mechanics in Many-Body Systems*, 2nd ed. (World Scientific, Singapore, 2008).

[53] R. A. Kendall, T. Dunning, Jr., and R. J. Harrison, Electron affinities of the first-row atoms revisited. systematic basis sets and wave functions, J. Chem. Phys. **96**, 6796 (1992).

[54] It is typically found here that it is only the energy of the highest occupied molecular orbital (HOMO) that is larger, at the *GW* level compared with HF, and that the MOs below the HOMO have smaller energies at *GW* level than HF and are thus more easily perturbed by the positron. This leads to an overall increase in the strength of the positron-molecule correlation potential and ultimately increased binding energies compared with the calculations that use the HF energies in the diagrams.

[55] D. G. Green and G. F. Gribakin, γ-ray spectra and enhancement factors for positron annihilation with core electrons, Phys. Rev. Lett. **114**, 093201 (2015).

[56] J. R. Danielson, S. Ghosh, and C. M. Surko, Influence of geometry on positron binding to molecules, J. Phys. B **54**, 225201 (2021).

[57] Y. Sugiura, T. Takayanagi, Y. Kita, and M. Tachikawa, Positron binding to hydrocarbon molecules: Calculation using the positron-electron correlation polarization potential, Eur. J. Phys. D **73**, 162 (2019).

[58] M. Tachikawa, Positron-attachment to acetonitrile, acetaldehyde, and acetone molecules: Vibrational enhancement of positron affinities with configuration interaction level of multicomponent molecular orbital approach, J. Phys.: Conf. Ser. **488**, 012053 (2014).

[59] V. K. Voora and K. D. Jordan, Nonvalence correlation-bound anion state of C_6F_6: Doorway to low-energy electron capture, J. Phys. Chem. A **118**, 7201 (2014).

[60] J. P. Rogers, C. S. Anstöter, and J. R. R. Verlet, Evidence of electron capture of an outgoing photoelectron wave by a nonvalence state in $(C_6F_6)_n-$, J. Phys. Chem. Lett. **9**, 2504 (2018).

[61] K. Iwata, R. G. Greaves, and C. M. Surko, Gamma-ray spectra from positron annihilation on atoms and molecules, Phys. Rev. A **55**, 3586 (1997).

[62] J. Romero, J. A. Charry, R. Flores-Moreno, M. T. do N. Varella, and A. Reyes, Calculation of positron binding energies using the generalized any particle propagator theory, J. Comput. Phys. **141**, 114103 (2014).

[63] F. A. Gianturco, J. Franz, R. J. Buenker, H.-P. Liebermann, L. Pichl, J.-M. Rost, M. Tachikawa, and M. Kimura, Positron binding to alkali-metal hydrides: The role of molecular vibrations, Phys. Rev. A **73**, 022705 (2006).

[64] R. J. Buenker and H.-P. Liebermann, Configuration interaction calculations of positron binding to molecular oxides and hydrides and its effect on spectroscopic constants, Nucl. Instrum. Methods Phys. Res. B **266**, 483 (2008).

[65] R. J. Buenker, H.-P. Liebermann, L. Pichl, M. Tachikawa, and M. Kimura, Role of the electric dipole moment in positron binding to the ground and excited states of the BeO molecule, J. Comput. Phys. **126**, 104305 (2007).

[66] E. Arthur-Baidoo, J. R. Danielson, C. M. Surko, J. P. Cassidy, S. K. Gregg, J. Hofierka, B. Cunningham, C. H. Patterson, and D. G. Green, "Positron annihilation and binding in aromatic and other ring molecules", https://doi.org/10.17034/56bb2190-fb92-4543-a171-36efa5872571 (2024).